

# New hexanuclear and octanuclear iron(III) oxide clusters: octahedral $[\text{Fe}_6\text{O}_2]^{14+}$ species and core isomerism in $[\text{Fe}_8\text{O}_4]^{16+}$ complexes

Euan K. Brechin<sup>a</sup>, Michael J. Knapp<sup>b</sup>, John C. Huffman<sup>a</sup>, David N. Hendrickson<sup>b,\*1</sup>,  
George Christou<sup>a,\*2</sup>

<sup>a</sup> Department of Chemistry and Molecular Structure Center, Indiana University, Bloomington, IN 47405-7102, USA

<sup>b</sup> Department of Chemistry, University of California at San Diego, La Jolla, CA 92093-0358, USA

Received 1 July 1999; accepted 20 August 1999

## Abstract

The synthesis, X-ray crystal structures and magnetic properties of two new classes of hexanuclear and octanuclear iron(III) clusters are reported. The reaction of hmpH (2-(hydroxymethyl)pyridine) with  $[\text{Fe}_3\text{O}(\text{O}_2\text{CR})_6(\text{H}_2\text{O})_3](\text{NO}_3)$  ( $\text{R} = \text{Bu}^t, \text{Ph}$ ) gives  $[\text{Fe}_6\text{O}_2(\text{O}_2\text{CR})_6(\text{hmp})_6](\text{NO}_3)_2$  containing a  $\text{Fe}_6^{\text{III}}$  octahedron with two opposite faces bridged by  $\mu_3\text{-O}^{2-}$  ions. Similar reactions employing  $\text{FeCl}_3/\text{NaO}_2\text{CR}$  ( $\text{R} = \text{Me}, \text{Ph}$ ) give  $[\text{Fe}_8\text{O}_4(\text{O}_2\text{CPh})_{11}(\text{hmp})_5]$  and  $[\text{Fe}_8\text{O}_4(\text{O}_2\text{CMe})_{12}(\text{hmp})_4]$ . Both contain a similar  $[\text{Fe}_8(\mu_3\text{-O})_4]$  core that can be described as four triangular  $[\text{Fe}_3\text{O}]$  units joined together by edge or vertex sharing or, alternatively, as two  $[\text{Fe}_3\text{O}]$  units bridged by a  $[\text{Fe}_2\text{O}_2]$  rhombus; however, the dispositions of the  $[\text{Fe}_3\text{O}]$  units about the  $[\text{Fe}_2\text{O}_2]$  central unit differ in the two complexes and can be described as *syn* and *anti* core isomers. The  $\text{Fe}_6$  and  $\text{Fe}_8$  complexes have been found to have  $S = 0$  ground states when studied by variable-temperature, solid-state magnetic susceptibility measurements, consistent with the expected antiferromagnetic exchange interactions between the Fe(III) ions. © 2000 Elsevier Science S.A. All rights reserved.

**Keywords:** Iron complexes; Polynuclear complexes; Magnetism; Crystal structures

## 1. Introduction

Polynuclear iron–oxo complexes have been of interest from a number of viewpoints. From a biological point of view, iron–oxo clusters of various sizes have represented model systems for the build up of the iron–oxo core of the iron storage protein ferritin [1,2], or for biomineralization processes that form a variety of iron–oxo minerals such as ferrihydrite, goethite, etc. [3]. Iron–oxo clusters have also been of interest from a materials point of view; discrete molecular species offer the potential of acting as precursors to molecule-based magnetic materials and even of functioning as nano-

scale magnetic particles themselves [4]. As a result of these and other stimuli, a wide variety of such clusters with aesthetically pleasing structures and interesting magnetic properties have been prepared and studied over the last 15 years or so [5–19].

The continuing development of the above areas requires the discovery of new examples on a regular basis, and we have thus been investigating new synthetic procedures capable of allowing access to new structural types. One approach has been to use appropriately chosen chelates to encourage aggregation while ensuring discrete products that are soluble and can be purified and crystallized. In this paper we describe the use of the anion of 2-(hydroxymethyl)pyridine ( $\text{hmp}^-$ ) in reaction systems that lead to  $\text{Fe}_6$  and  $\text{Fe}_8$  products that represent new structural types in iron–oxo cluster chemistry, and show that *syn*, *anti* core isomerism is possible for the  $\text{Fe}_8$  species.

<sup>1\*</sup> Corresponding author.

<sup>2\*</sup> Corresponding author. Tel./fax: +1-812-855-2399.

## 2. Experimental

### 2.1. Materials and characterization

Solvents were used as purchased, and reactions were performed under aerobic conditions.  $[\text{Fe}_3\text{O}(\text{O}_2\text{CR})_6(\text{H}_2\text{O})_3](\text{NO}_3)$  ( $\text{R} = \text{Bu}^t$  (**1**),  $\text{Ph}$  (**2**)) were prepared as previously described [20]. IR spectra (KBr) were recorded on a Nicolet 510P spectrophotometer.  $^1\text{H}$  NMR were recorded on a 300 MHz Varian Gemini 2000 spectrometer with the protio-solvent as a reference. Magnetic susceptibility measurements (d.c.) were carried out on powdered samples using a Quantum Design MPMS5 SQUID susceptometer equipped with a 55 kG magnet in a 10 kG applied field. Data were collected between 2 and 300 K. The samples were restrained in eicosane to prevent torquing. Pascal's constants were used to estimate the diamagnetic corrections, and they were subtracted from the experimental susceptibilities to give the molar paramagnetic susceptibilities.

### 2.2. Synthesis of $[\text{Fe}_6\text{O}_2(\text{O}_2\text{CBu}^t)_6(\text{hmp})_6](\text{NO}_3)_2$ (**3**)

A stirred solution of  $[\text{Fe}_3\text{O}(\text{O}_2\text{CBu}^t)_2(\text{H}_2\text{O})_3](\text{NO}_3)$  (0.500 g, 0.552 mmol) in MeCN (25 ml) was treated with solid hmpH (0.181 g, 1.66 mmol) to give a red-brown solution. This was left overnight at room temperature (r.t.), the solvent removed in vacuo, and the residue dissolved in  $\text{CHCl}_3$ . The solution was filtered, and the filtrate layered with equivolume  $\text{Et}_2\text{O}$  to give after several days dark red-brown crystals of  $3\cdot 4\text{CHCl}_3$  in ~50% yield based on Fe. Dried solid analyzed as solvent-free. *Anal.* Calc. for  $\text{C}_{66}\text{H}_{90}\text{Fe}_6\text{N}_8\text{O}_{26}$ : C, 45.39; H, 5.19; N, 6.42. Found: C, 45.45; H, 5.40; N, 6.12%. Selected IR data ( $\text{cm}^{-1}$ ): 1608(m), 1560(s), 1485(s), 1427(s), 1383(m), 1290(m), 1155(m), 1062(w), 1045(m), 1024(w), 898(w), 787(w), 765(w), 677(w), 661(w), 646(w), 596(m), 553(m), 509(w), 430(m).

### 2.3. Synthesis of $[\text{Fe}_6\text{O}_2(\text{O}_2\text{CPh})_6(\text{hmp})_6](\text{NO}_3)_2$ (**4**)

The previous procedure was employed with  $[\text{Fe}_3\text{O}(\text{O}_2\text{CPh})_2(\text{H}_2\text{O})_3](\text{NO}_3)$  (0.50 g, 0.49 mmol) and hmpH (0.160 g, 1.46 mmol). The  $\text{CHCl}_3/\text{Et}_2\text{O}$  crystallization system gave red-brown crystals of  $4\cdot 14\text{CHCl}_3\cdot \text{H}_2\text{O}$  in ~50% yield. Dried solid analyzed as  $4\cdot \text{H}_2\text{O}$ . *Anal.* Calc. for  $\text{C}_{78}\text{H}_{68}\text{Fe}_6\text{N}_8\text{O}_{27}$ : C, 49.71; H, 3.64; N, 5.95. Found: C, 49.53; H, 3.64; N, 5.78%.

### 2.4. Synthesis of $[\text{Fe}_8\text{O}_4(\text{O}_2\text{CPh})_{11}(\text{hmp})_5]$ (**5**)

$\text{FeCl}_3$  (0.500 g, 3.08 mmol),  $\text{NaO}_2\text{CPh}$  (0.887 g, 6.16 mmol), hmpH (0.672 g, 6.16 mmol) and NaOMe (0.333 g, 6.16 mmol) were dissolved with stirring in MeOH (25 ml) to give a red-brown solution. The solution was

maintained overnight at r.t., filtered, and the solvent then removed in vacuo. The solid was dissolved in  $\text{MeCO}_2\text{Et}/\text{Me}_2\text{CO}$  (2:1, 15 ml) and the solution allowed to stand undisturbed. Red-brown crystals grew over three days, and these were collected by filtration in ~50% yield. The solid can also be crystallized from MeCN.

An alternative procedure involves the reaction of  $(\text{NEt}_4)[\text{Fe}_2\text{OCl}_6]$  (0.500 g, 0.832 mmol),  $\text{NaO}_2\text{CPh}$  (0.240 g, 1.66 mmol) and hmpH (0.182 g, 1.66 mmol) in MeCN (25 ml) with stirring to give a red-brown solution which deposits a crystalline precipitate over 24 h. This was collected by filtration and recrystallized from  $\text{CH}_2\text{Cl}_2/\text{Et}_2\text{O}$ ,  $\text{CHCl}_3/\text{Et}_2\text{O}$ , or  $\text{CHCl}_3/\text{MeCN}/\text{pentane}$  as red-brown crystals in ~40% yield after two days. *Anal.* Calc. for  $\text{C}_{107}\text{H}_{85}\text{Fe}_8\text{N}_5\text{O}_{31}$ : C, 53.92; H, 3.59; N, 2.94. Found: C, 53.53; H, 3.66; N, 3.11%. Selected IR data ( $\text{cm}^{-1}$ ): 1599(s), 1549(s), 1491(w), 1402(vs), 1284(w), 1174(w), 1153(w), 1095(m), 1068(m), 1045(m), 1024(m), 761(m), 717(s).

### 2.5. Synthesis of $[\text{Fe}_8\text{O}_4(\text{O}_2\text{CMe})_{12}(\text{hmp})_4]$ (**6**)

$\text{FeCl}_3$  (0.500 g, 3.08 mmol),  $\text{NaO}_2\text{CMe}$  (0.506 g, 6.16 mmol) and  $\text{Na}(\text{hmp})$  (0.806 g, 6.16 mmol) were dissolved with stirring in MeOH (30 ml) to give a red-brown solution. The solution was maintained overnight at r.t., filtered, and the solvent removed in vacuo. The residue was dissolved in THF (10 ml) and allowed to stand undisturbed to give red-brown crystals in ~10% yield after a few days. Crystals were also obtained from  $\text{CH}_2\text{Cl}_2/\text{Et}_2\text{O}$  and  $\text{MeCO}_2\text{Et}/\text{Me}_2\text{CO}$  solutions. Selected IR data ( $\text{cm}^{-1}$ ): 1608(s), 1574(s), 1487(m), 1441(vs), 1379(s), 1344(m), 1321(m), 1294(m), 1223(w), 1157(w), 1095(s), 1049(s), 1022(m), 762(m), 721(s), 694(s), 663(s), 652(s), 540(m), 505(m), 472(m), 416(m).

### 2.6. X-ray crystallography

X-ray crystallographic data were collected on a Picker four-circle diffractometer at low temperature. Suitable crystals were affixed to the ends of glass fibers using silicone grease and transferred to the goniostat where they were cooled for characterization and data collection. Details of the diffractometry, low-temperature facilities, and computational procedures employed by the Molecular Structure Center are available elsewhere [21]. The structures were solved by direct methods (SHELXTL or MULTAN) and Fourier methods, and refined on  $F$  or  $F^2$  by full-matrix least-squares cycles.

#### 2.6.1. $[\text{Fe}_6\text{O}_2(\text{O}_2\text{CBu}^t)_6(\text{hmp})_6](\text{NO}_3)_2$ (**3**)

Complex  $3\cdot 4\text{CHCl}_3$  crystallizes in the monoclinic space group  $P2_1/n$ . The  $\text{Fe}_6$  cation lies on an inversion center. All non-hydrogen atoms of the cation, anion and  $\text{CHCl}_3$  solvate molecules were readily located and

refined anisotropically. Hydrogen atoms were included as fixed, isotropic contributors in the final refinement cycles with thermal parameters of 1.0 plus the isotropic equivalent of the parent atom. A final difference Fourier map was essentially featureless, with the largest peak being  $1.02 \text{ e } \text{Å}^{-3}$  in the vicinity of one of the  $\text{CHCl}_3$  molecules. Final  $R$  ( $R_w$ ) values are listed in Table 1.

#### 2.6.2. $[\text{Fe}_6\text{O}_2(\text{O}_2\text{CPh})_6(\text{hmp})_6](\text{NO}_3)_2$ (**4**)

Complex **4**· $14\text{CHCl}_3$ · $\text{H}_2\text{O}$  crystallizes in a triclinic space group. The  $\text{Fe}_6$  cation again lies on an inversion center. In addition to a  $\text{NO}_3^-$  anion, the asymmetric unit contains seven  $\text{CHCl}_3$  molecules, four well ordered but three disordered to various degrees. In addition, there was what appeared to be a  $\text{H}_2\text{O}$  molecule near an inversion center. An analytical absorption correction was performed. The non-hydrogen atoms of the cation, anion and four ordered  $\text{CHCl}_3$  molecules were refined anisotropically, the remainder were refined isotropically. Hydrogen atoms were added as fixed, isotropic

contributors as for **3**· $4\text{CHCl}_3$ . The final difference Fourier map was essentially featureless, the largest peak being  $1.8 \text{ e } \text{Å}^{-3}$  near a disordered  $\text{CHCl}_3$  molecule. Final  $R$  ( $R_w$ ) values are listed in Table 1.

#### 2.6.3. $[\text{Fe}_8\text{O}_4(\text{O}_2\text{CPh})_{11}(\text{hmp})_5]$ (**5**)

Complex **5**· $4.25\text{MeCN}$ · $2.71\text{CH}_2\text{Cl}_2$ · $\text{C}_5\text{H}_{12}$ · $0.62\text{H}_2\text{O}$  crystallizes in the triclinic space group with the  $\text{Fe}_8$  molecule in a general position. All non-hydrogen atoms of the  $\text{Fe}_8$  molecule were readily located and refined anisotropically; hydrogen atoms were included as fixed, isotropic contributors as for **3**· $4\text{CHCl}_3$ . The refinement was complicated by extensive amounts of solvent of crystallization, as indicated in the formula. The n-pentane, one  $\text{CH}_2\text{Cl}_2$  and three  $\text{MeCN}$  molecules have 100% occupancy, but the remaining two  $\text{MeCN}$ , five  $\text{CH}_2\text{Cl}_2$  and one  $\text{H}_2\text{O}$  molecules have occupancies of 66, 59, 64, 36, 34, 22, 15 and 62%, respectively, giving the total solvent content in the above formula. The final difference Fourier map was essentially featureless, with the largest peak being  $1.5 \text{ e } \text{Å}^{-3}$  near a disordered

Table 1

Crystallographic data for complexes **3**· $4\text{CHCl}_3$ , **4**· $14\text{CHCl}_3$ · $\text{H}_2\text{O}$ , **5**· $\text{solvent}$ <sup>a</sup>, and **6**· $12\text{THF}$

	<b>3</b>	<b>4</b>	<b>5</b>	<b>6</b>
Formula <sup>b</sup>	$\text{C}_{70}\text{H}_{94}\text{N}_8\text{O}_{26}\text{Cl}_{12}\text{Fe}_6$	$\text{C}_{92}\text{H}_{82}\text{N}_8\text{O}_{27}\text{Cl}_{42}\text{Fe}_6$	$\text{C}_{123.2}\text{H}_{116.4}\text{N}_{9.25}\text{O}_{31.6}\text{Cl}_{5.4}\text{Fe}_8$	$\text{C}_{96}\text{H}_{156}\text{N}_4\text{O}_{44}\text{Fe}_8$
Formula weight ( $\text{g mol}^{-1}$ )	2224.07	3555.80	2870.08	2517.13
Space group	$P2_1/n$	$P\bar{1}$	$P\bar{1}$	$C2/c$
$a$ (Å)	13.162(2)	14.217(3)	19.211(2)	25.393(5)
$b$ (Å)	25.243(4)	18.397(4)	23.587(2)	26.517(6)
$c$ (Å)	14.556(2)	14.170(3)	15.878(2)	17.046(3)
$\alpha$ (°)	90	111.96(1)	104.950(5)	90
$\beta$ (°)	104.21(1)	98.87(1)	97.305(5)	92.94(1)
$\gamma$ (°)	90	82.32(1)	108.217(5)	90
$V$ (Å <sup>3</sup> )	4688	3384	6417	11 462
$Z$	2	1	2	4
$T$ (°C)	−112	−167	−174	−172
Radiation (Å) <sup>c</sup>	0.71069	0.71069	0.71069	0.71069
$D_{\text{calc}}$ ( $\text{g cm}^{-3}$ )	1.576	1.745	1.485	1.459
$\mu$ ( $\text{cm}^{-1}$ )	13.187	15.216	10.69	10.620
Data range (°)	$6 \leq 2\theta \leq 50$	$6 \leq 2\theta \leq 50$	$6 \leq 2\theta \leq 50$	$6 \leq 2\theta \leq 50$
Data collected	$+h, +k, +l$	$+h, \pm k, \pm l$	$+h, \pm k, \pm l$	$+h, +k, \pm l$
Total data	9150	14 259	29 322	17 038
Unique data	8253	11 927	22 568	10 085
$R_{\text{merge}}$	0.124	0.041	0.041	0.176
Observed data	4834 <sup>d</sup>	8627 <sup>e</sup>	15 220 <sup>f</sup>	4615 <sup>d</sup>
$R$ ( $R_w$ ) (%) <sup>g,h</sup>	8.88 (5.97)	9.54 (9.80)	5.92 (14.6 <sup>i</sup> )	11.62 (8.22)
Goodness-of-fit <sup>j</sup>	1.661	2.096	1.231	1.525

<sup>a</sup>  $5 \cdot 4.25\text{MeCN} \cdot 2.71\text{CH}_2\text{Cl}_2 \cdot \text{C}_5\text{H}_{12} \cdot 0.62\text{H}_2\text{O}$ .

<sup>b</sup> Including solvate molecules.

<sup>c</sup> Graphite monochromator.

<sup>d</sup>  $F > 2.33\sigma(F)$ .

<sup>e</sup>  $F > 3.0\sigma(F)$ .

<sup>f</sup>  $F > 4\sigma(F)$ .

<sup>g</sup>  $R = 100 \sum ||F_o| - |F_c|| / \sum |F_o|$ .

<sup>h</sup>  $R_w = 100 [\sum w(|F_o| - |F_c|)^2 / \sum w|F_o|^2]^{0.5}$ , where  $w = 1/\sigma^2(|F_o|)$ .

<sup>i</sup>  $R_w(F^2) = 100 [\sum w(F_o^2 - F_c^2)^2 / \sum w(F_o^2)]^{0.5}$ .

<sup>j</sup>  $\text{GOF} = \{[\sum w(|F_o| - |F_c|)^2 / (n - p)]^{0.5}$ , where  $n$  = observed reflections and  $p$  = refined parameters.

$\text{CH}_2\text{Cl}_2$  molecule. Final  $R$ , and  $R_w(F^2)$  values are listed in Table 1.

#### 2.6.4. $[\text{Fe}_8\text{O}_4(\text{O}_2\text{CMe})_{12}(\text{hmp})_4]$ (**6**)

Complex **6**·12THF crystallizes in the monoclinic space group  $C2/c$  with the  $\text{Fe}_8$  molecule lying on a twofold rotation axis that passes through the central atom Fe(1) and Fe(2). The crystals lose THF molecules extremely rapidly and great care had to be exercised. All non-hydrogen atoms of the  $\text{Fe}_8$  molecule were readily located, and difference Fourier maps then revealed six THF molecules in the asymmetric unit. Four were well defined, and two suffered from very large thermal parameters. During the refinement, it was nearly impossible to achieve convergence while varying all parameters. While the  $\text{Fe}_8$  cluster is well defined and converged readily, it was necessary to fix the thermal parameters of one of the THF solvents to achieve convergence. In addition to the THF molecules, a single peak (O(78)) was located in a

void of over  $7 \text{ \AA}$  in diameter; it is probable that additional solvent should have been present at that location. The four well-behaved THF molecules were refined anisotropically to improve the model. Only the Fe atoms of the cluster were allowed to vary anisotropically. Hydrogen atoms were added in fixed, calculated positions as for  $3 \cdot 4\text{CH}_2\text{Cl}_2$ . A final difference Fourier map was featureless, the largest peak being  $1.21 \text{ e \AA}^{-3}$ . Final  $R$  ( $R_w$ ) values are listed in Table 1.

### 3. Results and discussion

#### 3.1. Synthesis of $[\text{Fe}_6\text{O}_2(\text{O}_2\text{CR})_6(\text{hmp})_6](\text{NO}_3)_2$ ( $R = \text{Bu}^t, \text{Ph}$ )

The  $R = \text{Bu}^t$  (**3**) and  $\text{Ph}$  (**4**) complexes were obtained in a similar fashion from the reaction of  $[\text{Fe}_3\text{O}-$

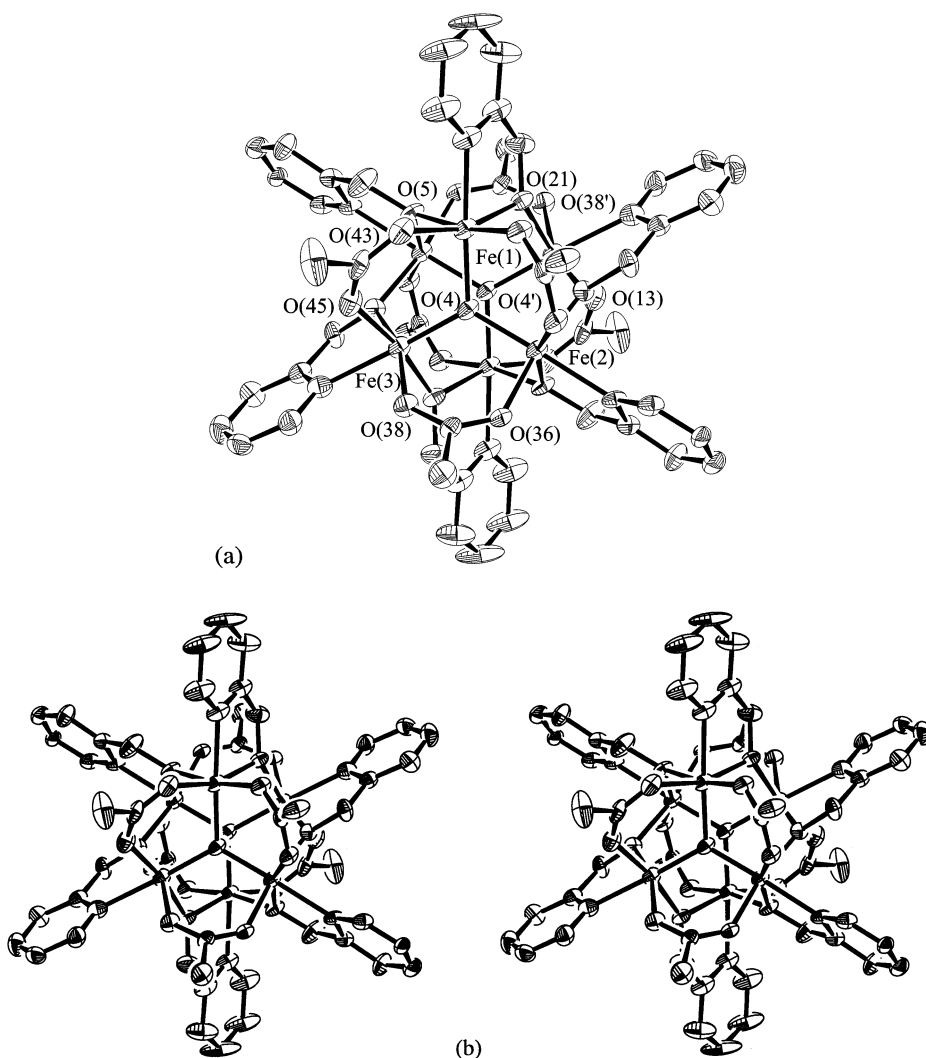
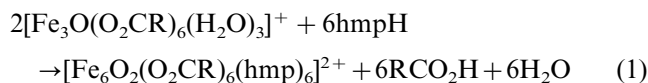


Fig. 1. Labeled ORTEP plot (a) and stereoview (b) at the 50% probability level of the  $[\text{Fe}_6\text{O}_2(\text{O}_2\text{CBu}^t)_6(\text{hmp})_6]^{2+}$  cation of **3**; the carboxylate Me groups have been omitted for clarity. The view is approximately along the  $S_6$  axis.

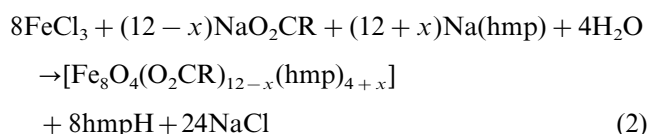
$(\text{O}_2\text{CR})_6(\text{H}_2\text{O})_3]^+$  with three equivalents of hmpH in MeCN. The procedures gave good yields (50%) of pure material after straightforward work-up, and they can be summarized as in Eq. (1).



Consideration of Eq. (1) and the structures of **3/4** and the  $[\text{Fe}_3\text{O}]^{7+}$  starting complexes **1** and **2** (vide infra) allow the conclusion that the hmp<sup>−</sup> groups have caused a dimerization of two  $[\text{Fe}_3\text{O}]^{7+}$  units in a face-to-face fashion with little change to the individual  $[\text{Fe}_3\text{O}]$  cores. The products of the two reactions are identical, i.e. the identity of the carboxylate has no effect on the reaction product, either in its overall formulation or its structural parameters to first order.

### 3.2. Synthesis of $[\text{Fe}_8\text{O}_4(\text{O}_2\text{CR})_{12-x}(\text{hmp})_{4+x}]$ ( $R = \text{Ph}, \text{Me}; x = 0, 1$ )

The two complexes with  $R = \text{Ph}$ ,  $x = 1$  and  $R = \text{Me}$ ,  $x = 0$ ,  $[\text{Fe}_8\text{O}_4(\text{O}_2\text{CPh})_{11}(\text{hmp})_5]$  (**5**) and  $[\text{Fe}_8\text{O}_4(\text{O}_2\text{CMe})_{12}(\text{hmp})_4]$  (**6**), respectively, were prepared in a similar fashion from the  $\text{FeCl}_3:\text{NaO}_2\text{CR}:\text{Na}(\text{hmp}) = 1:2:2$  reaction system in MeOH. This gave a good yield for **5** (50%) but a poor one for **6** (10%) after recrystallization. Both were found to crystallize in a suitable form for crystallography allowing the differences in formulation and core structure (vide infra) to be determined with accuracy: there is a slight difference in formulation, with **5** containing an extra hmp<sup>−</sup> and one less  $\text{RCO}_2^-$  groups than **6**, and a difference in the  $\text{Fe}_6$  topology of the cores. Whether the latter is the cause or the effect of the former is not clear. It is even possible that several species are in equilibrium in solution for both the  $R = \text{Ph}$  and  $\text{Me}$  systems and that what are obtained in the crystalline forms differ merely due to differing relative solubilities, crystallization kinetics, and other, medium-dependent properties. It should be noted, however, that several crystallization systems were explored for **5** before strongly-diffracting crystals were obtained from  $\text{CH}_2\text{Cl}_2/\text{MeCN}/\text{pentane}$ . In these other cases, crystal structures were solved to the point of compound identification, and in every case, the product was identical to **5** (including for crystals grown from  $\text{MeCO}_2\text{Et}/\text{Me}_2\text{CO}$  where the formula was  $[\text{Fe}_8\text{O}_4(\text{O}_2\text{CPh})_{10}(\text{O}_2\text{CMe})(\text{hmp})_5]$ , the monodentate  $\text{PhCO}_2^-$  group being replaced by  $\text{MeCO}_2^-$  presumably originating from the ethyl acetate). The formations of **5** and **6** can be summarized in Eq. (2).



### 3.3. Structural description of $[\text{Fe}_6\text{O}_2(\text{O}_2\text{CBu}')_6(\text{hmp})_6]^{2+}$ ( $\text{NO}_3$ )<sub>2</sub> (**3**) and $[\text{Fe}_6\text{O}_2(\text{O}_2\text{CPh})_6(\text{hmp})_6]$ (**4**)

A labeled ORTEP plot and stereoview of the cation of **3** are presented in Fig. 1, and selected bond distances and angles are listed in Table 2. The structure of the cation of **4** is extremely similar to that of **3** and is thus not described separately: a comparison of the averaged structural parameters of the two cations is provided in Table 3 and full structural detail for **4** is available in Section 5.

The cation of **3** consists of two  $[\text{Fe}_3(\mu_3\text{-O})]^{7+}$  triangular units held together in a face-to-face fashion by six bridging hmp<sup>−</sup> groups. Each  $\eta^1:\eta^2:\mu\text{-hmp}^-$  group chelates an Fe atom and bridges with its O atom to an Fe atom in the neighboring  $[\text{Fe}_3\text{O}]$  unit. Each Fe⋯Fe pair within a  $[\text{Fe}_3\text{O}]$  unit is additionally bridged by a  $\text{Bu}'\text{CO}_2^-$  group, completing six-coordinate, near octahedral geometry at each metal. The cation has crystal-

Table 2

Selected bond distances (Å) and angles (°) for  $[\text{Fe}_6\text{O}_2(\text{O}_2\text{CBu}')_6(\text{hmp})_6](\text{NO}_3)_2 \cdot 4\text{CH}_2\text{Cl}_2$  (**3**·4CH<sub>2</sub>Cl<sub>2</sub>)

Fe(1)–Fe(2)	3.348(3)	Fe(2)–O(4)	1.919(6)
Fe(1)–Fe(3)	3.328(3)	Fe(2)–O(5)	2.002(6)
Fe(2)–Fe(3)	3.358(2)	Fe(2)–O(13)	2.011(6)
Fe(1)–Fe(2')	3.489(3)	Fe(2)–O(31)	2.032(6)
Fe(1)–Fe(3')	3.470(3)	Fe(2)–O(36)	2.017(6)
Fe(2)–Fe(3')	3.456(3)	Fe(2)–N(12)	2.166(7)
Fe(1)–O(4)	1.945(6)	Fe(3)–O(4)	1.933(6)
Fe(1)–O(5)	2.038(5)	Fe(3)–O(13)	2.007(5)
Fe(1)–O(21)	2.019(6)	Fe(3)–O(21)	2.022(6)
Fe(1)–O(29)	2.030(6)	Fe(3)–O(38)	2.018(5)
Fe(1)–O(43)	2.027(7)	Fe(3)–O(45)	2.012(7)
Fe(1)–N(28)	2.186(8)	Fe(3)–N(20)	2.180(8)
O(4)–Fe(1)–O(5)	95.22(22)	O(29)–Fe(1)–O(43)	84.75(25)
O(4)–Fe(1)–O(21)	102.12(25)	O(29)–Fe(1)–N(28)	82.07(25)
O(4)–Fe(1)–O(29)	94.22(23)	O(43)–Fe(1)–N(28)	84.5(3)
O(4)–Fe(1)–O(43)	96.10(25)	O(4)–Fe(2)–O(5)	102.09(23)
O(4)–Fe(1)–N(28)	176.18(25)	O(4)–Fe(2)–O(13)	94.72(24)
O(5)–Fe(1)–O(21)	83.46(23)	O(4)–Fe(2)–O(31)	95.44(23)
O(5)–Fe(1)–O(29)	170.46(23)	O(4)–Fe(2)–O(36)	94.19(24)
O(5)–Fe(1)–O(43)	92.84(24)	O(4)–Fe(2)–N(12)	178.08(26)
O(5)–Fe(1)–N(28)	88.52(24)	O(5)–Fe(2)–O(13)	84.03(23)
O(21)–Fe(1)–O(29)	95.93(25)	O(5)–Fe(2)–O(31)	162.27(23)
O(21)–Fe(1)–O(43)	161.65(25)	O(5)–Fe(2)–O(36)	96.21(24)
O(21)–Fe(1)–N(28)	77.49(28)	O(5)–Fe(2)–N(12)	77.62(24)
O(13)–Fe(2)–O(31)	91.96(23)	O(13)–Fe(3)–O(45)	95.85(24)
O(13)–Fe(2)–O(36)	170.83(23)	O(13)–Fe(3)–N(20)	77.99(26)
O(13)–Fe(2)–N(12)	87.14(25)	O(21)–Fe(3)–O(38)	92.45(24)
O(31)–Fe(2)–O(36)	85.04(24)	O(21)–Fe(3)–O(45)	170.17(26)
O(31)–Fe(2)–N(12)	84.95(25)	O(21)–Fe(3)–N(20)	89.04(26)
O(36)–Fe(2)–N(12)	83.96(25)	O(38)–Fe(3)–O(45)	85.99(25)
O(4)–Fe(3)–O(13)	104.02(23)	O(38)–Fe(3)–N(20)	84.32(26)
O(4)–Fe(3)–O(21)	95.06(23)	O(45)–Fe(3)–N(20)	81.16(28)
O(4)–Fe(3)–O(38)	93.96(23)	Fe(1)–O(4)–Fe(2)	120.1(3)
O(4)–Fe(3)–O(45)	94.73(25)	Fe(1)–O(4)–Fe(3)	118.2(3)
O(4)–Fe(3)–N(20)	175.63(27)	Fe(2)–O(4)–Fe(3)	121.3(3)
O(13)–Fe(3)–O(21)	82.63(23)	Fe(1)–O(5)–Fe(2)	119.4(3)
O(13)–Fe(3)–O(38)	161.68(24)		

Table 3  
Comparison of selected bond distances (Å) and angles (°) <sup>a</sup> in  
[Fe<sub>6</sub>O<sub>2</sub>(O<sub>2</sub>CR)<sub>6</sub>(hmp)<sub>6</sub>](NO<sub>3</sub>)<sub>2</sub> (R = Bu<sup>t</sup> (**3**), Ph (**4**))

Parameter	<b>3</b>	<b>4</b>
Fe...Fe <sup>b</sup>	3.345(3)	3.348(3)
Fe...Fe <sup>c</sup>	3.472(3)	3.487(3)
Fe–O <sub>i</sub>	1.932(6)	1.934(6)
Fe–O <sub>b</sub> <sup>d</sup>	2.009(6)	2.014(6)
Fe–O <sub>b</sub> <sup>e</sup>	2.024(6)	2.023(6)
Fe–O <sub>i</sub> –Fe	119.9(3)	119.9(3)
Fe–O <sub>b</sub> –Fe	118.8(3)	119.5(3)
O <sub>i</sub> –Fe–O <sub>b</sub> <sup>d</sup>	102.74(23)	102.60(23)
O <sub>i</sub> –Fe–O <sub>b</sub> <sup>e</sup>	95.00(23)	95.25(23)
O <sub>b</sub> –Fe–O <sub>b</sub>	83.37(23)	83.02(23)

<sup>a</sup> Averaged under idealized *S*<sub>6</sub> symmetry; numbers in parentheses are the e.s.d. of individual values.

<sup>b</sup> Within an [Fe<sub>3</sub>(μ<sub>3</sub>-O)] unit.

<sup>c</sup> Between [Fe<sub>3</sub>(μ<sub>3</sub>-O)] units.

<sup>d</sup> Within an Fe/hmp chelate ring.

<sup>e</sup> Not within an Fe/hmp chelate ring.

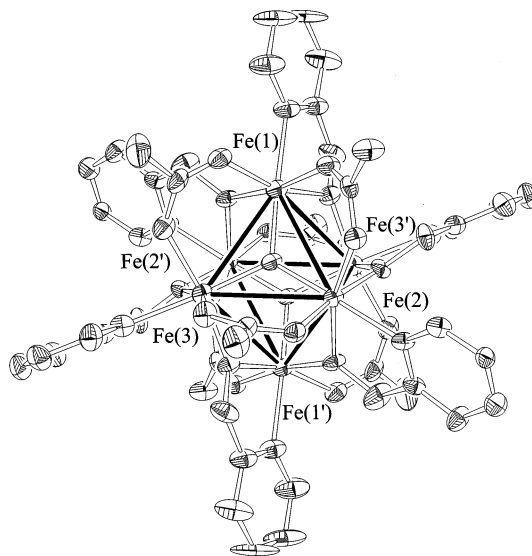


Fig. 2. ORTEP plot of the cation of **3** showing the Fe...Fe vectors to emphasize the Fe<sub>6</sub> octahedron.

lographic *C*<sub>i</sub> symmetry, but virtual *S*<sub>6</sub> symmetry with the *S*<sub>6</sub> axis passing through the μ<sub>3</sub>-O<sup>2-</sup> atom O(4) and its symmetry-related partner. The disposition of the two [Fe<sub>3</sub>O] units gives an octahedral Fe<sub>6</sub> topology, emphasized in Fig. 2 by inclusion of Fe...Fe vectors. From this alternative viewpoint, the cation may be described as an Fe<sub>6</sub> octahedron with two opposite faces bridged by μ<sub>3</sub>-O<sup>2-</sup> ions and six edges bridged by μ-O(hmp) atoms. Despite this variety of bridges, however, the Fe<sub>6</sub> octahedron is only slightly distorted: Fe...Fe separations within the [Fe<sub>3</sub>O] units (average 3.345 Å) are only

slightly shorter than the rest (average 3.472 Å). The non-adjacent Fe...Fe separations are much longer (average 4.833 Å).

The structure of the cation of **4** is very similar to that of **3** showing that the different carboxylate has little influence on the core. Consideration of the structural parameters in Table 3, averaged under effective *S*<sub>6</sub> symmetry, shows differences that are statistically insignificant, and the cations are thus isostructural.

Complexes **3** and **4** join only a small number of other hexanuclear Fe(III) complexes that contain an Fe<sub>6</sub> octa-

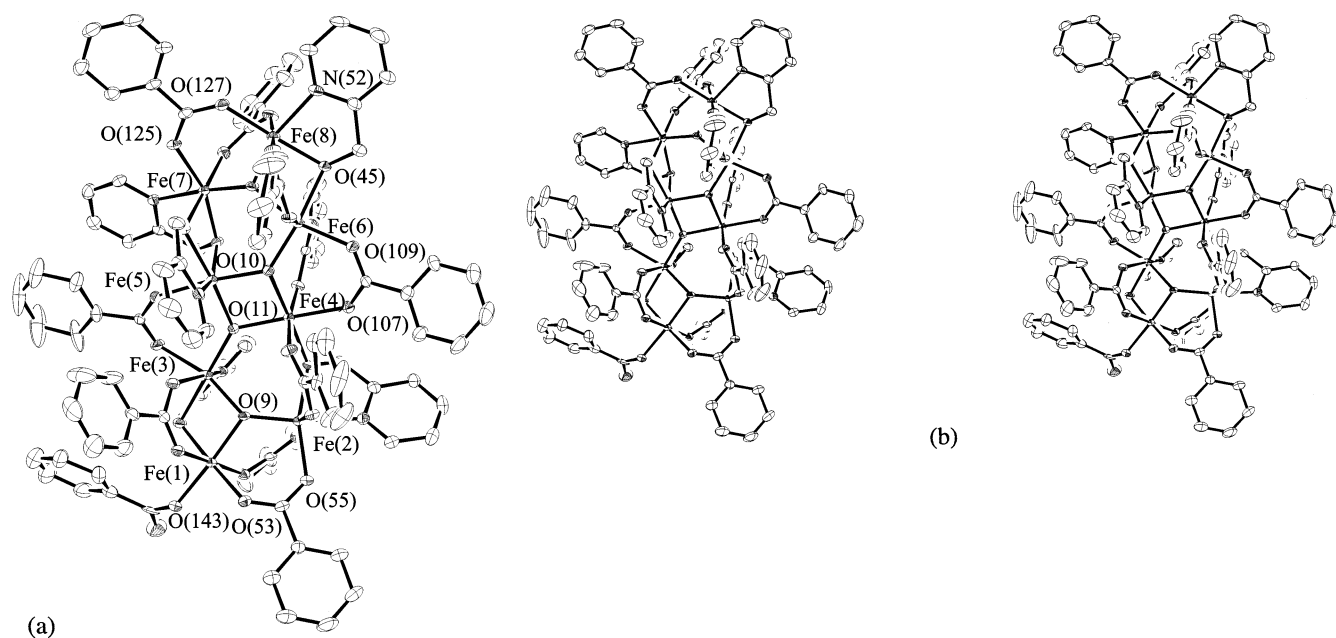


Fig. 3. Labeled ORTEP plot (a) and stereoview (b) of [Fe<sub>8</sub>O<sub>4</sub>(O<sub>2</sub>CPh)<sub>11</sub>(hmp)<sub>5</sub>] (**5**) at the 50% probability level.

hedron. These comprise the  $[\text{Fe}_6\text{O}(\text{OMe})_{18}]^{2-}$  [18],  $[\text{Fe}_6\text{O}(\text{L}_3)_6]^{2-}$  [17] and  $[\text{Fe}_6\text{O}(\text{L}_3)_3(\text{OMe})_3\text{Cl}_6]^{2-}$  [17] clusters, where  $\text{L}_3$  is a polyolato ligand. In these previously reported species, the core is more symmetrical than that in **3** and **4**, consisting of an  $\text{Fe}_6$  octahedron at the center of which is a  $\mu_6\text{-O}^{2-}$  ion and which has an alkoxide-like O atom bridging each of the twelve  $\text{Fe}_2$  edges, i.e. effectively a  $[\text{Fe}_6(\mu_6\text{-O})(\mu\text{-OR})_{12}]$  core with virtual  $O_h$  core symmetry.

### 3.4. Structural description of $[\text{Fe}_8\text{O}_4(\text{O}_2\text{CPh})_{11}(\text{hmp})_5]$ (**5**)

A labeled ORTEP plot and stereoview are presented in Fig. 3, and selected distances and angles are listed in Table 4. The complex contains a  $[\text{Fe}_8(\mu_3\text{-O})_4]^{16+}$  core that can be described as comprising four linked  $[\text{Fe}_3(\mu_3\text{-O})]^{7+}$  triangular units, as can be more clearly seen in Fig. 4 (a): edge-fusion of two such units at common atoms Fe(4) and Fe(5) gives an  $[\text{Fe}_4(\mu_3\text{-O})_2]$

Table 4  
Selected bond distances (Å) and angles (°) for  $\text{Fe}_8\text{O}_4(\text{O}_2\text{CPh})_{11}(\text{hmp})_5 \cdot \text{solv}$  (**5**-solv)

Fe(1)–Fe(3)	2.976(1)	Fe(4)–O(107)	2.076(3)
Fe(4)–Fe(5)	2.898(1)	Fe(5)–O(10)	1.945(3)
Fe(6)–Fe(8)	2.976(1)	Fe(5)–O(11)	1.951(3)
Fe(1)–Fe(2)	3.287(1)	Fe(4)–Fe(6)	3.306(1)
Fe(2)–Fe(3)	3.487(1)	Fe(5)–Fe(6)	3.473(1)
Fe(3)–Fe(4)	3.484(1)	Fe(5)–Fe(7)	3.075(1)
Fe(3)–Fe(5)	3.443(1)	Fe(6)–Fe(7)	3.524(1)
Fe(2)–Fe(4)	3.502(1)	Fe(7)–Fe(8)	3.243(1)
Fe(1)–O(9)	1.968(3)	Fe(5)–O(37)	2.037(3)
Fe(1)–O(143)	1.968(3)	Fe(5)–O(91)	2.044(3)
Fe(1)–O(13)	1.987(3)	Fe(5)–O(29)	2.046(3)
Fe(1)–O(53)	2.019(3)	Fe(5)–N(44)	2.165(4)
Fe(1)–O(62)	2.051(3)	Fe(6)–O(11)	1.857(3)
Fe(1)–O(71)	2.060(3)	Fe(6)–O(12)	1.974(3)
Fe(2)–O(9)	1.842(3)	Fe(6)–O(109)	2.030(3)
Fe(2)–O(21)	2.011(3)	Fe(6)–O(100)	2.037(3)
Fe(2)–O(55)	2.052(3)	Fe(6)–O(116)	2.050(3)
Fe(2)–O(80)	2.052(3)	Fe(6)–O(45)	2.079(3)
Fe(2)–O(64)	2.061(3)	Fe(7)–O(12)	1.838(3)
Fe(2)–N(28)	2.201(4)	Fe(7)–O(37)	1.978(3)
Fe(3)–O(10)	1.866(3)	Fe(7)–O(29)	2.009(3)
Fe(3)–O(9)	1.954(3)	Fe(7)–O(125)	2.046(3)
Fe(3)–O(73)	2.035(3)	Fe(7)–O(134)	2.066(3)
Fe(3)–O(13)	2.052(3)	Fe(7)–N(36)	2.188(4)
Fe(3)–O(89)	2.085(3)	Fe(8)–O(12)	1.865(3)
Fe(3)–N(20)	2.174(4)	Fe(8)–O(45)	1.983(3)
Fe(4)–O(11)	1.925(3)	Fe(8)–O(127)	2.027(3)
Fe(4)–O(10)	1.942(3)	Fe(8)–O(136)	2.050(3)
Fe(4)–O(21)	2.032(3)	Fe(8)–O(118)	2.073(3)
Fe(4)–O(82)	2.032(3)	Fe(8)–N(52)	2.114(4)
Fe(4)–O(98)	2.052(3)		
O(9)–Fe(1)–O(143)	175.33(15)	O(9)–Fe(2)–N(28)	172.56(14)
O(9)–Fe(1)–O(13)	82.12(13)	O(21)–Fe(2)–N(28)	76.55(14)
O(143)–Fe(1)–O(13)	93.26(14)	O(55)–Fe(2)–N(28)	85.36(14)
O(9)–Fe(1)–O(53)	94.72(13)	O(80)–Fe(2)–N(28)	83.42(14)
O(143)–Fe(1)–O(53)	89.91(14)	O(64)–Fe(2)–N(28)	86.19(14)
O(13)–Fe(1)–O(53)	176.72(14)	O(10)–Fe(3)–O(9)	100.87(13)

Table 4 (Continued)

O(9)–Fe(1)–O(62)	90.15(13)	O(10)–Fe(3)–O(73)	98.08(14)
O(143)–Fe(1)–O(62)	89.25(14)	O(9)–Fe(3)–O(73)	90.48(13)
O(13)–Fe(1)–O(62)	90.83(14)	O(10)–Fe(3)–O(13)	175.10(14)
O(53)–Fe(1)–O(62)	90.06(14)	O(9)–Fe(3)–O(13)	80.80(13)
O(9)–Fe(1)–O(71)	89.46(13)	O(73)–Fe(3)–O(13)	86.48(13)
O(143)–Fe(1)–O(71)	91.23(14)	O(10)–Fe(3)–O(89)	94.68(13)
O(13)–Fe(1)–O(71)	90.28(14)	O(9)–Fe(3)–O(89)	163.77(13)
O(53)–Fe(1)–O(71)	88.80(14)	O(73)–Fe(3)–O(89)	82.73(14)
O(62)–Fe(1)–O(71)	178.76(14)	O(13)–Fe(3)–O(89)	84.07(13)
O(9)–Fe(2)–O(21)	96.02(13)	O(10)–Fe(3)–N(20)	98.33(14)
O(9)–Fe(2)–O(55)	102.08(13)	O(9)–Fe(3)–N(20)	100.50(14)
O(21)–Fe(2)–O(55)	161.23(13)	O(73)–Fe(3)–N(20)	158.13(15)
O(9)–Fe(2)–O(80)	97.50(14)	O(13)–Fe(3)–N(20)	76.81(14)
O(21)–Fe(2)–O(80)	99.10(13)	O(89)–Fe(3)–N(20)	81.61(14)
O(55)–Fe(2)–O(80)	83.52(13)	O(11)–Fe(4)–O(10)	83.71(13)
O(9)–Fe(2)–O(64)	94.06(13)	O(11)–Fe(4)–O(21)	176.27(14)
O(21)–Fe(2)–O(64)	87.87(13)	O(10)–Fe(4)–O(21)	93.97(13)
O(55)–Fe(2)–O(64)	85.97(13)	O(11)–Fe(4)–O(82)	91.57(13)
O(80)–Fe(2)–O(64)	165.77(13)	O(10)–Fe(4)–O(82)	92.78(14)
O(21)–Fe(4)–O(82)	91.45(13)	O(37)–Fe(7)–O(125)	90.64(13)
O(11)–Fe(4)–O(98)	91.49(13)	O(29)–Fe(7)–O(125)	162.38(14)
O(10)–Fe(4)–O(98)	95.79(13)	O(12)–Fe(7)–O(134)	91.84(14)
O(21)–Fe(4)–O(98)	85.84(12)	O(37)–Fe(7)–O(134)	176.88(14)
O(82)–Fe(4)–O(98)	171.16(14)	O(29)–Fe(7)–O(134)	98.68(13)
O(11)–Fe(4)–O(107)	95.43(13)	O(125)–Fe(7)–O(134)	90.65(14)
O(10)–Fe(4)–O(107)	175.98(14)	O(12)–Fe(7)–N(36)	171.63(15)
O(21)–Fe(4)–O(107)	87.08(12)	O(37)–Fe(7)–N(36)	91.80(14)
O(82)–Fe(4)–O(107)	83.31(14)	O(29)–Fe(7)–N(36)	76.66(14)
O(98)–Fe(4)–O(107)	88.15(13)	O(125)–Fe(7)–N(36)	89.32(14)
O(10)–Fe(5)–O(11)	82.94(13)	O(134)–Fe(7)–N(36)	85.37(14)
O(10)–Fe(5)–O(37)	173.13(14)	O(12)–Fe(8)–O(45)	82.21(13)
O(11)–Fe(5)–O(37)	103.38(13)	O(12)–Fe(8)–O(127)	101.20(14)
O(10)–Fe(5)–O(91)	91.41(13)	O(45)–Fe(8)–O(127)	173.84(14)
O(11)–Fe(5)–O(91)	173.25(13)	O(12)–Fe(8)–O(136)	92.37(14)
O(37)–Fe(5)–O(91)	82.45(13)	O(45)–Fe(8)–O(136)	97.73(14)
O(10)–Fe(5)–O(29)	100.40(13)	O(127)–Fe(8)–O(136)	87.31(14)
O(11)–Fe(5)–O(29)	90.02(13)	O(12)–Fe(8)–O(118)	94.00(14)
O(37)–Fe(5)–O(29)	77.14(13)	O(45)–Fe(8)–O(118)	89.54(13)
O(91)–Fe(5)–O(29)	94.64(13)	O(127)–Fe(8)–O(118)	85.12(14)
O(10)–Fe(5)–N(44)	106.85(15)	O(136)–Fe(8)–O(118)	170.92(13)
O(11)–Fe(5)–N(44)	90.27(14)	O(12)–Fe(8)–N(52)	160.47(15)
O(37)–Fe(5)–N(44)	76.13(14)	O(45)–Fe(8)–N(52)	78.39(14)
O(91)–Fe(5)–N(44)	87.84(15)	O(127)–Fe(8)–N(52)	98.33(15)
O(29)–Fe(5)–N(44)	152.57(14)	O(136)–Fe(8)–N(52)	88.00(15)
O(11)–Fe(6)–O(12)	96.00(13)	O(118)–Fe(8)–N(52)	88.15(15)
O(11)–Fe(6)–O(109)	99.04(13)	Fe(2)–O(9)–Fe(3)	133.45(17)
O(12)–Fe(6)–O(109)	164.03(13)	Fe(2)–O(9)–Fe(1)	119.21(15)
O(11)–Fe(6)–O(100)	93.35(13)	Fe(3)–O(9)–Fe(1)	98.72(14)
O(12)–Fe(6)–O(100)	93.15(13)	Fe(3)–O(10)–Fe(4)	132.41(16)
O(109)–Fe(6)–O(100)	91.29(14)	Fe(3)–O(10)–Fe(5)	129.23(17)
O(11)–Fe(6)–O(116)	92.60(13)	Fe(4)–O(10)–Fe(5)	96.45(13)
O(12)–Fe(6)–O(116)	89.41(13)	Fe(6)–O(11)–Fe(4)	121.85(17)
O(109)–Fe(6)–O(116)	84.61(13)	Fe(6)–O(11)–Fe(5)	131.52(17)
O(100)–Fe(6)–O(116)	173.25(13)	Fe(4)–O(11)–Fe(5)	96.77(13)
O(11)–Fe(6)–O(45)	173.19(14)	Fe(7)–O(12)–Fe(8)	122.26(17)
O(12)–Fe(6)–O(45)	77.27(12)	Fe(7)–O(12)–Fe(6)	135.16(16)
O(109)–Fe(6)–O(45)	87.76(13)	Fe(8)–O(12)–Fe(6)	101.61(15)
O(100)–Fe(6)–O(45)	86.09(13)	Fe(1)–O(13)–Fe(3)	94.90(14)
O(116)–Fe(6)–O(45)	88.39(13)	Fe(2)–O(21)–Fe(4)	120.03(15)
O(12)–Fe(7)–O(37)	90.78(14)	Fe(7)–O(29)–Fe(5)	98.63(14)
O(12)–Fe(7)–O(29)	96.00(13)	Fe(7)–O(37)–Fe(5)	99.95(14)
O(37)–Fe(7)–O(29)	79.35(13)	Fe(8)–O(45)–Fe(6)	94.23(13)
O(12)–Fe(7)–O(125)	98.61(14)		

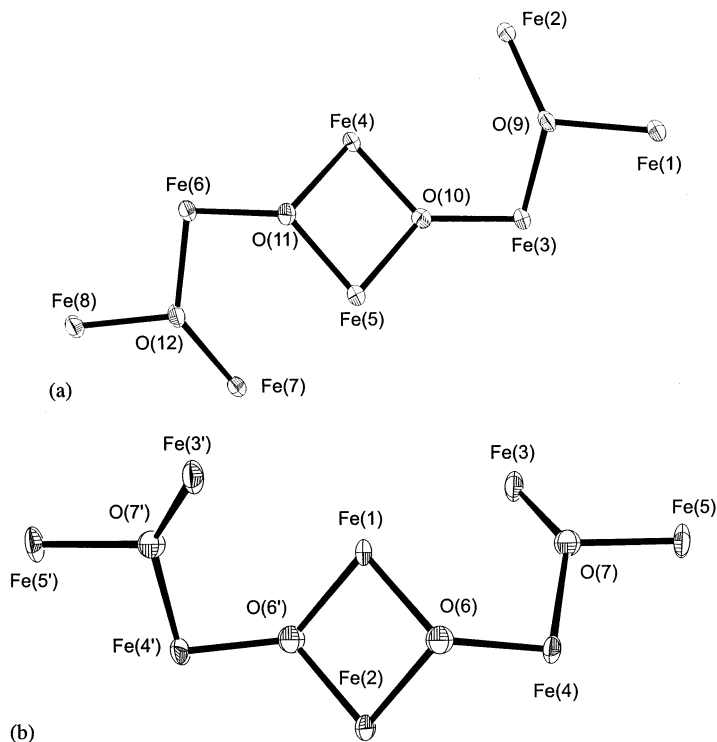


Fig. 4. Comparison of the  $[\text{Fe}_8\text{O}_4]^{16+}$  cores of  $[\text{Fe}_8\text{O}_4(\text{O}_2\text{CPh})_{11}(\text{hmp})_3]$  (**5**) (a) and  $[\text{Fe}_8\text{O}_4(\text{O}_2\text{CMe})_{12}(\text{hmp})_4]$  (**6**) (b) emphasizing the *anti* and *syn* topologies, respectively.

unit as found in tetranuclear complexes such as  $[\text{Fe}_4\text{O}_2(\text{O}_2\text{CMe})_7(\text{bpy})_2](\text{ClO}_4)$  ( $\text{bpy} = 2,2'$ -bipyridine) [22] and  $(\text{N}^n\text{Bu}_4)[\text{Fe}_4\text{O}_2(\text{O}_2\text{CMe})_7(\text{pic})_2]$  ( $\text{pic} = 2$ -picolinate) [23]. Vertex-fusion of the  $[\text{Fe}_4\text{O}_2]$  unit with two additional  $[\text{Fe}_3\text{O}]$  units at common atoms Fe(3) and Fe(6) gives the final  $[\text{Fe}_8\text{O}_4]^{16+}$  core: the disposition of the terminal  $[\text{Fe}_3\text{O}]$  units about the central unit is *anti*. Alternatively, the  $[\text{Fe}_8\text{O}_4]$  core can be described as two  $[\text{Fe}_3\text{O}]^{7+}$  units connected by a bridging  $[\text{Fe}_2\text{O}_2]$  rhombus. Peripheral ligation to the core is provided by eleven  $\text{PhCO}_2^-$  and five  $\text{hmp}^-$  groups. Ten of the  $\text{PhCO}_2^-$  groups are in their familiar  $\eta^1:\eta^1:\mu$ -bridging modes and one is terminally coordinated to Fe(1). The  $\text{hmp}^-$  groups all chelate one Fe atom and bridge to a second Fe atom with their O atoms, as in complexes **3** and **4**.  $\text{Fe}\cdots\text{Fe}$  separations bridged by two O atoms, either from two oxide ions ( $\text{Fe}(4)\cdots\text{Fe}(5) = 2.898(1) \text{ \AA}$ ) or one oxide and one  $\text{hmp}^-$  O ( $\text{Fe}(1)\cdots\text{Fe}(3) = 2.976(1) \text{ \AA}$  and  $\text{Fe}(6)\cdots\text{Fe}(8) = 2.976 \text{ \AA}$ ) are  $< 3 \text{ \AA}$ , whilst other  $\text{Fe}\cdots\text{Fe}$  separations are  $> 3 \text{ \AA}$  (see Table 4). As expected, the  $\text{Fe}-\text{O}^{2-}$  bonds ( $1.838(3)$ – $1.974(3) \text{ \AA}$ ) are all shorter than any of the other  $\text{Fe}-\text{O}$  bonds in the molecule, with the exception of the terminal benzoate group ( $\text{Fe}(1)-\text{O}(143) = 1.968(3) \text{ \AA}$ ).

### 3.5. Structural description of $[\text{Fe}_8\text{O}_4(\text{O}_2\text{CMe})_{12}(\text{hmp})_4]$ (**6**)

A labeled ORTEP and stereoview are presented in Fig. 5, and selected distances and angles are listed in Table

5. The complex contains a  $[\text{Fe}_8(\mu_3\text{-O})_4]^{16+}$  core that is related to that in **5**, but with some notable differences. It can be again described as four connected  $[\text{Fe}_3\text{O}]$  units or, alternatively, as two  $[\text{Fe}_3\text{O}]$  units bridged by a  $[\text{Fe}_2\text{O}_2]$  rhombus, but now the two terminal  $[\text{Fe}_3\text{O}]$  units are *syn* about the central unit. This is emphasized in Fig. 4, where the core of **6** is compared with that of **5**. As far as the cores are concerned, the complexes are thus *syn*, *anti* isomers. As for **5**,  $\text{Fe}\cdots\text{Fe}$  separations fall into two types,  $< 3 \text{ \AA}$  for those bridged by two O atoms, and  $> 3 \text{ \AA}$  for those bridged by one O atom. Unlike **5**, however, there are now twelve carboxylate groups, all in bridging modes, and four  $\text{hmp}^-$  groups, again in a chelating/bridging mode. Complex **6** is consequently of much higher symmetry than **5**, possessing crystallographic  $C_2$  symmetry, the  $C_2$  axis passing through Fe(1) and Fe(2), whereas **5** has no crystallographic (or virtual) symmetry elements. Again, the  $\text{Fe}-\text{O}^{2-}$  bonds are the shortest in the molecule, except for  $\text{Fe}(4)-\text{O}(7)$ , which is unusually long at  $2.015(10) \text{ \AA}$ .

### 3.6. Magnetochemistry

Variable-temperature, solid-state magnetic susceptibility studies were performed in a 1 Tesla (10 kOe) field in the temperature range 2.00–300 K. Complexes **3** and **4** gave essentially identical results and only those for the former will be described.

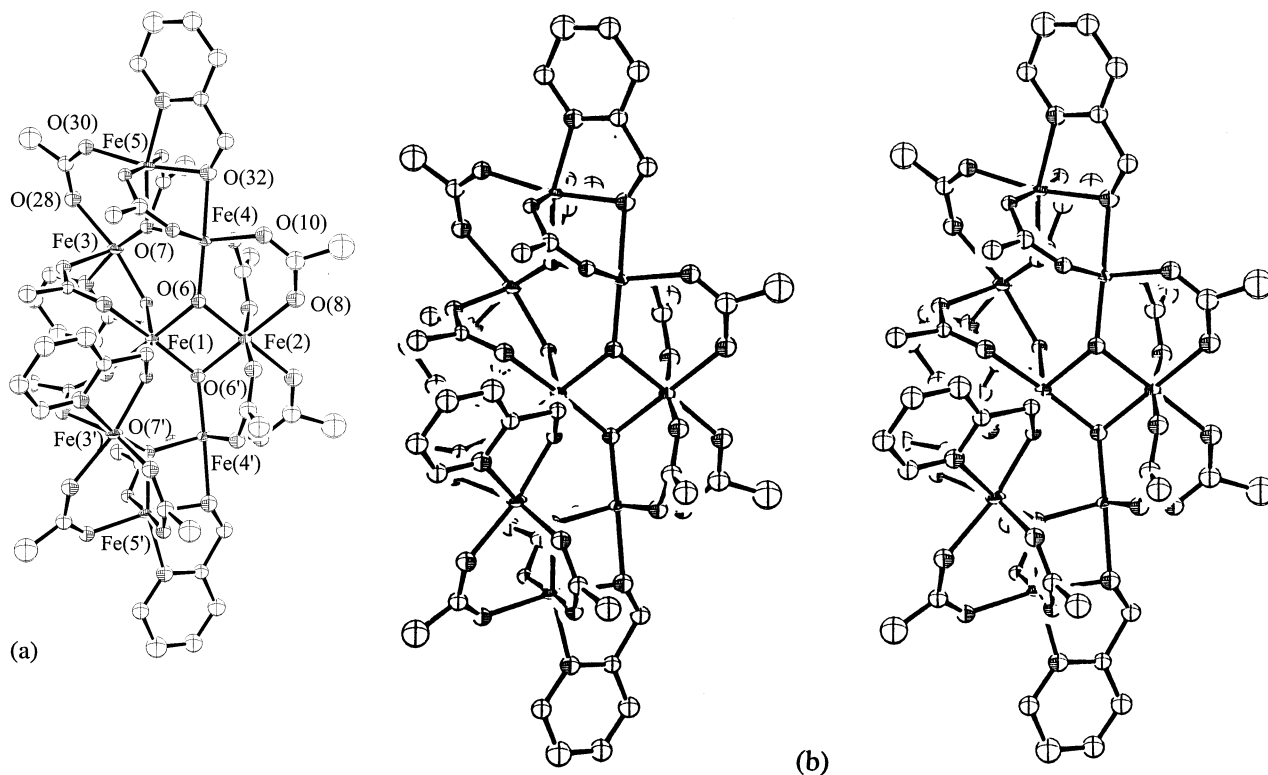


Fig. 5. Labeled ORTEP plot (a) and stereoview (b) of  $[\text{Fe}_8\text{O}_4(\text{O}_2\text{CMe})_{12}(\text{hmp})_4]$  (**6**) at the 50% probability level. Primed and unprimed atoms are related by a  $C_2$  axis.

Table 5  
Selected bond distances (Å) and angles (°) for  $[\text{Fe}_8\text{O}_4(\text{O}_2\text{CMe})_{12}(\text{hmp})_4] \cdot 12\text{THF}$  (**6**·12THF)

Fe(1)–Fe(2)	2.864(5)	Fe(3)–O(28)	2.100(11)
Fe(1)–Fe(3)	3.486(5)	Fe(3)–O(40)	1.967(9)
Fe(1)–Fe(4)	3.446(5)	Fe(3)–N(47)	2.171(12)
Fe(2)–Fe(4)	3.302(5)	Fe(4)–O(6)	1.857(9)
Fe(3)–Fe(4)	3.562(5)	Fe(4)–O(7)	2.015(10)
Fe(3)–Fe(5)	3.168(5)	Fe(4)–O(10)	2.009(11)
Fe(4)–Fe(5)	2.963(5)	Fe(4)–O(14)	2.060(10)
Fe(1)–O(6)	1.941(10)	Fe(4)–O(24)	2.079(9)
Fe(1)–O(16)	2.042(10)	Fe(4)–O(32)	2.079(10)
Fe(1)–O(40)	2.068(9)	Fe(5)–O(7)	1.882(9)
Fe(2)–O(6)	1.957(10)	Fe(5)–O(22)	2.055(10)
Fe(2)–O(8)	2.075(11)	Fe(5)–O(26)	2.069(9)
Fe(2)–O(12)	2.018(10)	Fe(5)–O(30)	2.017(11)
Fe(3)–O(7)	1.806(9)	Fe(5)–O(32)	1.969(11)
Fe(3)–O(18)	2.062(10)	Fe(5)–N(39)	2.150(12)
Fe(3)–O(20)	2.043(11)		
O(6)–Fe(1)–O(6)	85.9(6)	O(16)–Fe(1)–O(40)	80.5(4)
O(6)–Fe(1)–O(16)	93.5(4)	O(16)–Fe(1)–O(40)	92.4(4)
O(6)–Fe(1)–O(16)	171.7(4)	O(40)–Fe(1)–O(40)	170.1(6)
O(6)–Fe(1)–O(16)	93.5(4)	O(6)–Fe(2)–O(6)	85.0(6)
O(6)–Fe(1)–O(40)	95.9(4)	O(6)–Fe(2)–O(8)	94.4(4)
O(6)–Fe(1)–O(40)	91.4(4)	O(6)–Fe(2)–O(8)	179.1(4)
O(6)–Fe(1)–O(40)	95.9(4)	O(6)–Fe(2)–O(8)	94.4(4)
O(6)–Fe(1)–O(40)	91.4(4)	O(6)–Fe(2)–O(8)	179.1(4)
O(16)–Fe(1)–O(16)	88.2(6)	O(6)–Fe(2)–O(12)	95.4(4)
O(16)–Fe(1)–O(40)	92.4(4)	O(6)–Fe(2)–O(12)	92.5(4)
O(6)–Fe(2)–O(12)	95.4(4)	O(10)–Fe(4)–O(14)	89.0(4)

Table 5 (continued)

O(8)–Fe(2)–O(8)	86.2(6)	O(10)–Fe(4)–O(24)	90.6(4)
O(8)–Fe(2)–O(12)	88.2(4)	O(10)–Fe(4)–O(32)	84.1(4)
O(8)–Fe(2)–O(12)	84.0(4)	O(14)–Fe(4)–O(24)	171.0(4)
O(8)–Fe(2)–O(12)	88.2(4)	O(14)–Fe(4)–O(32)	84.6(4)
O(12)–Fe(2)–O(12)	169.3(7)	O(24)–Fe(4)–O(32)	86.4(4)
O(7)–Fe(3)–O(18)	96.3(4)	O(7)–Fe(5)–O(22)	91.4(4)
O(7)–Fe(3)–O(20)	92.7(4)	O(7)–Fe(5)–O(26)	89.0(4)
O(7)–Fe(3)–O(28)	102.1(4)	O(7)–Fe(5)–O(30)	105.4(4)
O(7)–Fe(3)–O(40)	92.7(4)	O(7)–Fe(5)–O(32)	85.1(4)
O(7)–Fe(3)–N(47)	170.1(5)	O(7)–Fe(5)–N(39)	162.0(5)
O(18)–Fe(3)–O(20)	161.1(4)	O(22)–Fe(5)–O(26)	175.4(4)
O(18)–Fe(3)–O(28)	79.9(4)	O(22)–Fe(5)–O(30)	86.4(4)
O(18)–Fe(3)–O(40)	97.8(4)	O(22)–Fe(5)–O(32)	92.2(4)
O(18)–Fe(3)–N(47)	86.5(4)	O(22)–Fe(5)–N(39)	95.5(4)
O(20)–Fe(3)–O(28)	82.0(4)	O(26)–Fe(5)–O(30)	89.0(4)
O(20)–Fe(3)–O(40)	98.3(4)	O(26)–Fe(5)–O(32)	92.4(4)
O(20)–Fe(3)–N(47)	87.5(4)	O(26)–Fe(5)–N(39)	85.5(4)
O(28)–Fe(3)–O(40)	165.3(4)	O(30)–Fe(5)–O(32)	169.5(4)
O(28)–Fe(3)–N(47)	87.7(5)	O(30)–Fe(5)–N(39)	91.6(5)
O(40)–Fe(3)–N(47)	77.6(4)	O(32)–Fe(5)–N(39)	78.1(5)
O(6)–Fe(4)–O(7)	99.5(4)	Fe(1)–O(6)–Fe(2)	94.6(4)
O(6)–Fe(4)–O(10)	97.3(4)	Fe(1)–O(6)–Fe(4)	130.2(6)
O(6)–Fe(4)–O(14)	96.7(4)	Fe(2)–O(6)–Fe(4)	119.9(5)
O(6)–Fe(4)–O(24)	92.3(4)	Fe(3)–O(7)–Fe(4)	137.5(5)
O(6)–Fe(4)–O(32)	178.0(5)	Fe(3)–O(7)–Fe(5)	118.4(5)
O(7)–Fe(4)–O(10)	163.1(4)	Fe(4)–O(7)–Fe(5)	99.0(4)
O(7)–Fe(4)–O(14)	90.1(4)	Fe(4)–O(32)–Fe(5)	94.0(4)
O(7)–Fe(4)–O(24)	87.7(4)	Fe(1)–O(40)–Fe(3)	119.5(4)
O(7)–Fe(4)–O(32)	79.0(4)		

For complex **3**, the effective magnetic moment ( $\mu_{\text{eff}}$ ) per  $\text{Fe}_6$  cluster steadily decreases from  $7.30 \mu_{\text{B}}$  at 300 K to  $0.987 \mu_{\text{B}}$  at 2.00 K (Fig. 6). The 300 K value may be compared to the  $\mu_{\text{eff}}$  value of  $14.49 \mu_{\text{B}}$  for a cluster of six non-interacting  $\text{Fe(III)}$  ( $S = 5/2$ ) ions with  $g = 2.00$ , indicating that the  $\text{Fe(III)}$  ions are interacting antiferromagnetically. The behavior with decreasing temperature and the  $\mu_{\text{eff}}$  value at 2.00 K are indicative of a  $S = 0$  ground state. This value is not surprising given that a spin singlet ground state is by far the most commonly observed situation in clusters containing an even number of  $\text{Fe(III)}$  ions, and where the exchange interactions are antiferromagnetic in nature [5–23]. In particular, the previous examples of species containing an  $\text{Fe}_6^{\text{III}}$  octahedron have also possessed an  $S = 0$  ground state [17,18], although, as described above, they possess a  $\mu_6\text{-O}^{2-}$  at the center of the octahedron and are thus not magnetically congruent with complex **3**. The data for **4** are almost superimposable on those of **3**, the  $\mu_{\text{eff}}$  value decreasing steadily from  $7.61 \mu_{\text{B}}$  at 300 K to  $1.36 \mu_{\text{B}}$  at 2.00 K.

For complex **5**, the  $\mu_{\text{eff}}$  value steadily decreases from  $8.31 \mu_{\text{B}}$  at 300 K to  $0.954 \mu_{\text{B}}$  at 2.00 K (Fig. 7). Again the 300 K value is much smaller than that expected for eight non-interacting  $\text{Fe(III)}$  ions with  $g = 2.00$  ( $16.7 \mu_{\text{B}}$ ) indicating the presence of appreciable antiferromagnetic exchange interactions. The variable-temperature data and the  $\mu_{\text{eff}}$  value at 2.00 K indicate that **5** also has a  $S = 0$  ground state. As for **3**, this is not unexpected: note that the central  $[\text{Fe}_4\text{O}_2]$  unit of **5** has been found to have a  $S = 0$  ground state in the discrete complexes  $[\text{Fe}_4\text{O}_2(\text{O}_2\text{CMe})_7(\text{bpy})_2]^+$  [22] and  $[\text{Fe}_4\text{O}_2(\text{O}_2\text{CMe})_7\text{z}(\text{pic})_2]^-$  [23], so with hindsight it is not unreasonable that the extended core of **5** similarly is  $S = 0$  in the ground state although it had been hoped that competing exchange interactions and spin frustration effects might have led to a nonzero ground state. Complex **6** was not investigated magnetochemically; notwithstanding the *syn* versus *anti* isomeric difference in the cores of **5** and **6**, the ground state of **6** is also expected to be  $S = 0$ . Unfortunately, it proved difficult to obtain **6** in sufficient quantities and purity for such studies.

#### 4. Conclusions

The use of the anion of 2-(hydroxymethyl)pyridine in reactions with  $\text{Fe(III)}$  reagents has allowed access to two new structural types in  $\text{Fe(III)}$  cluster chemistry, namely the  $[\text{Fe}_6(\mu_3\text{-O})_2]$  and  $[\text{Fe}_8(\mu_3\text{-O})_4]$  cores. The former contains an  $\text{Fe}_6$  octahedron with two opposite faces bridged by  $\text{O}^{2-}$  ions, while the latter contains a central  $[\text{Fe}_4(\mu_3\text{-O})_2]$  unit to which are fused two  $[\text{Fe}_3(\mu\text{-O})]$  units by vertex sharing. The latter also displays a *syn*, *anti* core isomerism in the two complexes **5** and **6**.

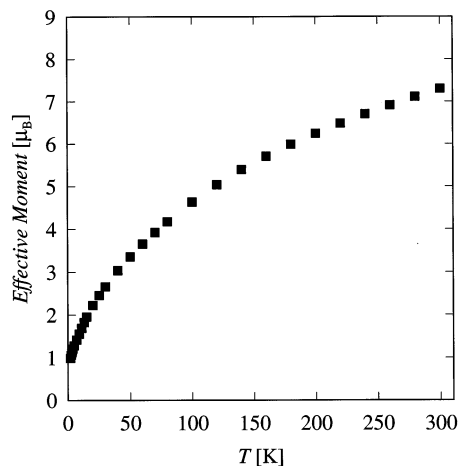


Fig. 6. Plot of effective magnetic moment ( $\mu_{\text{eff}}$ ) vs. temperature for  $[\text{Fe}_6\text{O}_2(\text{O}_2\text{Cbu}^t)_6(\text{hmp})_6](\text{NO}_3)_2$  (**3**).

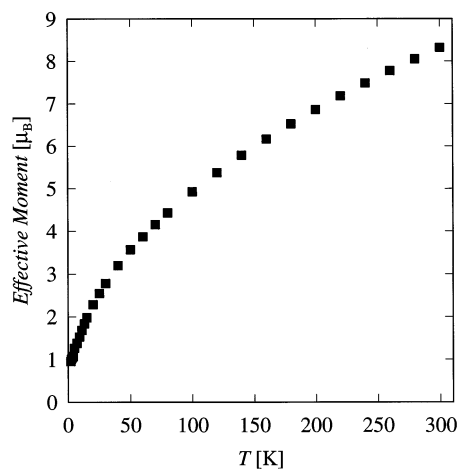


Fig. 7. Plot of effective magnetic moment ( $\mu_{\text{eff}}$ ) vs. temperature for  $[\text{Fe}_8\text{O}_4(\text{O}_2\text{CPh})_{11}(\text{hmp})_5]$  (**5**).

As is normally observed in  $\text{Fe(III)}_x$  clusters when  $x$  is even, complexes **3**, **4** and **5** possess  $S = 0$  ground states as a result of antiferromagnetic exchange interactions between the  $\text{Fe(III)}$  ( $S = 5/2$ ) ions.

The present work extends the body of results that emphasizes the ability of  $\text{hmp}^-$  to yield a variety of new structural types in Fe and Mn chemistry [24], and additional species with both these metals are currently in hand and will be reported in due course.

#### 5. Supplementary material

Crystallographic information in CIF format for complexes **3**–**6** has been deposited at the Cambridge Crystallographic Data Centre and may be retrieved using deposition numbers 125995 (**3**), 125996 (**4**), 125997 (**5**) and 125998 (**6**).

## Acknowledgements

This work was supported by NSF Grants to G.C. and D.N.H.

## References

- [1] E.C. Theil, *Annu. Rev. Biochem.* 56 (1987) 289 and Refs. cited therein.
- [2] B. Xu, D.J. Chasteen, *J. Biol. Chem.* 266 (1991) 19965.
- [3] S. Mann, J. Webb, R.J.P. Williams (Eds.), *Biom mineralization: Chemical and Biochemical Perspectives*, VCH, New York, 1988.
- [4] (a) A.-L. Barra, P. Debrunner, D. Gatteschi, C.E. Schulz, R. Sessoli, *Europhys. Lett.* 35 (1996) 133. (b) A. Caneschi, T. Ohm, C. Paulsen, D. Rovai, C. Sangregorio, R. Sessoli, *J. Magn. Magn. Mater.* 177–181 (1998) 1330.
- [5] (a) K. Wieghardt, K. Pohl, I. Jibril, G. Huttner, *Angew. Chem., Int. Ed. Engl.* 24 (1984) 77. (b) K.L. Taft, G.C. Papaefthymiou, S.J. Lippard, *Inorg. Chem.* 33 (1994) 1510.
- [6] (a) S.M. Gorun, G.C. Papaefthymiou, R.B. Frankel, S.J. Lippard, *J. Am. Chem. Soc.* 109 (1987) 3337. (b) W. Micklitz, V. McKee, R.L. Rardin, L.E. Pence, G.C. Papaefthymiou, S.G. Bott, S.J. Lippard, *J. Am. Chem. Soc.* 116 (1994) 8061.
- [7] A.K. Powell, S.L. Heath, D. Gatteschi, L. Pardi, R. Sessoli, G. Spina, F. Del Giallo, F. Pieralli, *J. Am. Chem. Soc.* 117 (1995) 2491.
- [8] V.S. Nair, K.S. Hagen, *Inorg. Chem.* 33 (1994) 185.
- [9] T. Tokii, K. Ide, M. Nakashima, M. Koikawa, *Chem. Lett.* (1994) 441.
- [10] (a) W. Micklitz, S.J. Lippard, *Inorg. Chem.* 27 (1988) 3069. (b) W. Micklitz, S.G. Bott, J.G. Bentsen, S.J. Lippard, *J. Am. Chem. Soc.* 111 (1989) 372.
- [11] A. Caneschi, A. Cornia, A.C. Fabretti, D. Gatteschi, *Angew. Chem., Int. Ed. Engl.* 34 (1995) 2716.
- [12] J.K. McCusker, C.A. Christmas, P.M. Hagen, R.K. Chadha, D.F. Harvey, D.N. Hendrickson, *J. Am. Chem. Soc.* 113 (1991) 6114.
- [13] V.S. Nair, K.S. Hagen, *Inorg. Chem.* 31 (1992) 4048.
- [14] (a) K.L. Taft, S.J. Lippard, *J. Am. Chem. Soc.* 112 (1990) 9629. (b) S.P. Watton, P. Fuhrmann, L.E. Pence, A. Caneschi, A. Cornia, G.L. Abbati, S.J. Lippard, *Angew. Chem., Int. Ed. Engl.* 36 (1997) 2774.
- [15] G.L. Abbati, A. Cornia, A.C. Fabretti, W. Malavasi, L. Schenetti, A. Caneschi, D. Gatteschi, *Inorg. Chem.* 36 (1997) 6443.
- [16] C. Benelli, S. Parsons, G.A. Solan, R.E.P. Winpenny, *Angew. Chem., Int. Ed. Engl.* 35 (1996) 1825.
- [17] (a) K. Hegetschweiler, H. Schmalle, H.M. Streit, W. Schneider, *Inorg. Chem.* 29 (1990) 3625. (b) A. Cornia, D. Gatteschi, K. Hegetschweiler, L. Hausherr-Primo, V. Gramlich, *Inorg. Chem.* 35 (1996) 4414.
- [18] K. Hegetschweiler, H.W. Schmalle, H.M. Streit, V. Gramlich, H.-U. Hund, I. Erni, *Inorg. Chem.* 31 (1992) 1299.
- [19] C.M. Grant, M.J. Knapp, W.E. Streib, J.C. Huffman, D.N. Hendrickson, G. Christou, *Inorg. Chem.* 37 (1998) 6065.
- [20] A. Earnshaw, B.N. Figgis, J. Lewis, *J. Chem. Soc. (A)* (1966) 1656.
- [21] M.H. Chisholm, K. Folting, J.C. Huffman, C.C. Kirkpatrick, *Inorg. Chem.* 23 (1984) 1021.
- [22] J.K. McCusker, J.B. Vincent, E.A. Schmitt, M.L. Mino, K. Shin, D.K. Coggin, P.M. Hagen, J.C. Huffman, G. Christou, D.N. Hendrickson, *J. Am. Chem. Soc.* 113 (1991) 3012.
- [23] M.K. Wemple, D.K. Coggin, J.B. Vincent, J.K. McCusker, W.E. Streib, J.C. Huffman, D.N. Hendrickson, G. Christou, *J. Chem. Soc., Dalton Trans.* (1998) 719.
- [24] M.A. Bolcar, S.M.J. Aubin, K. Folting, D.N. Hendrickson, G. Christou, *Chem. Commun.* (1997) 1485.